NEURAL REGENERATION RESEARCH
www.nrronline.org

Research Article

Withaferin A inhibits ferroptosis and protects against intracerebral hemorrhage

Zi-Xian Zhou[1, 2, #], Qi Cui[1, 2, #], Ying-Mei Zhang[1, 2], Jia-Xin Yang[1, 2], Wen-Jing Xiang[1, 2], Ning Tian[1, 3], Yan-Lin Jiang[4], Mei-Ling Chen[2], Bin Yang[3], Qing-Hua Li[1, 2, 3], Ru-Jia Liao[1, 2, 3, *]

https://doi.org/10.4103/1673-5374.355822

Date of submission: March 4, 2022

Date of decision: April 26, 2022

Date of acceptance: May 28, 2022

Date of web publication: September 15, 2022

From the Contents

Graphical Abstract

Withaferin A (WFA) application inhibits ferroptosis and attenuates oxidative stress-related damage after hemorrhagic stroke in in vivo and in vitro models and these effects are at least partially related to enhanced nuclear factor E2-related factor 2 (Nrf2) translocation and heme oxygenase-1 (HO-1) expression.

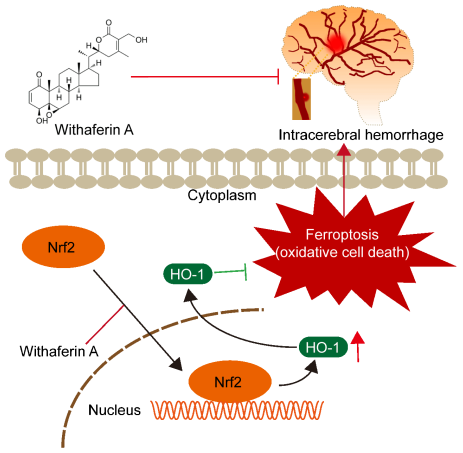

Abstract

Recent studies have indicated that suppressing oxidative stress and ferroptosis can considerably improve the prognosis of intracerebral hemorrhage (ICH). Withaferin A (WFA), a natural compound, exhibits a positive effect on a number of neurological diseases. However, the effects of WFA on oxidative stress and ferroptosis-mediated signaling pathways to ICH remain unknown. In this study, we investigated the neuroprotective effects and underlying mechanism for WFA in the regulation of ICH-induced oxidative stress and ferroptosis. We established a mouse model of ICH by injection of autologous tail artery blood into the caudate nucleus and an *in vitro* cell model of hemin-induced ICH. WFA was injected intracerebroventricularly at 0.1, 1 or 5 μg/kg once daily for 7 days, starting immediately after ICH operation. WFA markedly reduced brain tissue injury and iron deposition and improved neurological function in a dose-dependent manner 7 days after cerebral hemorrhage. Through *in vitro* experiments, cell viability test showed that WFA protected SH-SY5Y neuronal cells against hemin-induced cell injury. Enzyme-linked immunosorbent assays *in vitro* and *in vivo* showed that WFA markedly decreased the level of malondialdehyde, an oxidative stress marker, and increased the activities of anti-oxidative stress markers superoxide dismutase and glutathione peroxidase after ICH. Western blot assay, quantitative polymerase chain reaction and immunofluorescence results demonstrated that WFA activated the nuclear factor E2-related factor 2 (Nrf2)/heme oxygenase-1 (HO-1) signaling axis, promoted translocation of Nrf2 from the cytoplasm to nucleus, and increased HO-1 expression. Silencing Nrf2 with siRNA completely reversed HO-1 expression, oxidative stress and protective effects of WFA. Furthermore, WFA reduced hemin-induced ferroptosis. However, after treatment with an HO-1 inhibitor, the neuroprotective effects of WFA against hemin-induced ferroptosis were weakened. MTT test results showed that WFA combined with ferrostatin-1 reduced hemin-induced SH-SY5Y neuronal cell injury. Our findings reveal that WFA treatment alleviated ICH injury-induced ferroptosis and oxidative stress through activating the Nrf2/HO-1 pathway, which may highlight a potential role of WFA for the treatment of ICH.

Key Words: behavior; brain injuries; hemorrhagic stroke; ferroptosis; heme oxygenase-1; neuroprotection; nuclear factor E2-related factor 2; nuclear translocator; oxidative stress; stroke

Introduction

Intracerebral hemorrhage (ICH) is a subtype of stroke with high mortality and morbidity (Yang et al., 2016; Sorensen, 2019; Feigin et al., 2020; Collaborators, 2021). Primary injury directly caused by the hemorrhage together with secondary injury resulting from blood cytotoxicity, excitotoxicity, oxidative damage, and inflammation leads to severe disability or death (Xue and Yong, 2020). Therefore, ICH represents a serious issue to human health. Oxidative damage, which is caused by an imbalance between the production of reactive oxygen species (ROS) and efficient elimination of ROS by recovery enzymes, plays a pivotal role in the poor prognosis of ICH (Xie et al., 2020). Heme oxygenase-1 (HO-1), a limiting enzyme for heme catabolism and iron production, is induced by several stress factors such as oxidative stress and hypoxia (Chau, 2015; Chen et al., 2019b). HO-1 expression in the brain is either absent or extremely low under physiologically normal circumstances. In contrast, HO-1 expression greatly increases throughout ICH, and suppression of HO-1 in ICH has a remarkable therapeutic benefit (Wang and Dore, 2007; Zhang et al., 2017). HO-1 may thus be a potential therapeutic target for ICH.

Our previous study revealed that withaferin A (WFA), a bio-active steroid lactone derived from Withania somnifera (L.) Dunal (Solanaceae), inhibited the apoptosis of endothelial cells and modulated microglial activation after traumatic brain injury (Zhou et al., 2020). A recent report demonstrated that WFA exhibits a protective role in Parkinson's disease via regulating the DJ1-Nrf2-STING axis (Zhao et al., 2021). In addition, WFA treatment results in strong upregulation of the expression of HO-1 both in endothelial and microglial cells (Heyninck et al., 2016). However, the role of WFA in ICH remains unclear.

[1]Laboratory of Neuroscience, Affiliated Hospital of Guilin Medical University, Guilin Medical University, Guilin, Guangxi Zhuang Autonomous Region, China; [2]Department of Neurology, Affiliated Hospital of Guilin Medical University, Guilin Medical University, Guilin, Guangxi Zhuang Autonomous Region, China; [3]Guangxi Clinical Research Center for Neurological Diseases, Affiliated Hospital of Guilin Medical University, Guilin Medical University, Guilin, Guangxi Zhuang Autonomous Region, China; [4]Department of Pharmacology, Affiliated Hospital of Guilin Medical University, Guilin Medical University, Guilin, Guangxi Zhuang Autonomous Region, China

*Correspondence to: Ru-Jia Liao, PhD, liaorujia@hotmail.com.

https://orcid.org/0000-0001-6928-4003 (Ru-Jia Liao)

#Both authors contributed equally to this work.

Funding: *This work was supported by the Natural Science Foundation of Guangxi Zhuang Autonomous Region, No. 2020GXNSFAA259036 (to RJL); the Guangxi Science and Technology Project, No. Guike AD17129015 (to QHL); Guangxi Research and Innovation Base for Basic and Clinical Application of Nerve Injury and Repair Project, No. Guike ZY21195042 (to QHL); the Innovation Projects of Guangxi Graduate Education, Nos. YCSW2021246 (to ZXZ), YCSW2021254 (to WJX).*

How to cite this article: *Zhou ZX, Cui Q, Zhang YM, Yang JX, Xiang WJ, Tian N, Jiang YL, Chen ML, Yang B, Li QH, Liao RJ (2023) Withaferin A inhibits ferroptosis and protects against intracerebral hemorrhage. Neural Regen Res 18(6):1308-1315.*

Ferroptosis is a recently identified form of oxidative cell death, and ferroptosis inhibition has shown short- and long-term neuroprotective effects post-ICH (Chen et al., 2019a; Bao et al., 2020). Therefore, ferroptosis is a new target for ICH treatment (Wan et al., 2019; Bai et al., 2020). Notably, upregulation of HO-1 has been shown to mitigate ferroptosis and has a protective effect on intestinal ischemia/reperfusion, type 2 diabetic osteoporosis, and acute kidney injury (Fernandez-Mendivil et al., 2021). However, whether HO-1 potentiates ferroptosis in brain hemorrhagic condition or is induced as a protective response remains unclear.

While studies suggest that WFA inhibits ferroptosis, the exact underlying mechanism remains unknown. This study aimed to evaluate the neuroprotection and anti-ferroptosis effects of WFA by activating the Nrf2/HO-1 signaling pathway. Our results may help identify potential therapeutic targets for clinical therapy of ICH.

Methods

Animals

All animal experiments were approved by the Animal Experimentation Committee of Guilin Medical University (approval No. GLMC202003006, approval date: December 3, 2020) and were performed following the National Institutes of Health Guide for the Care and Use of Laboratory Animals. Considerable precautions were made to reduce the number of mice used for experiments. C57BL/6J mice (20 ± 2 g, 8–12 weeks old) were purchased from Hunan SJA Laboratory Animal Co., Ltd. (No. 43004700056305; Changsha, China). To reduce the effects of estrogen and its receptor on ICH, only adult male mice were used.

Experimental groups

Eighty-nine mice were used in this study. Mice were randomly divided into five groups: sham group (n = 21, 0.9% saline, intraperitoneal injection), ICH group (n = 21, 0.9% saline, intraperitoneal injection), and three ICH + WFA groups (ICH + WFA 0.1 μg/kg, n = 13; ICH + WFA 1 μg/kg, n = 21; ICH + WFA 5 μg/kg, n = 13; W4394, Sigma Aldrich, MO, USA). The dosing of WFA was chosen from earlier studies with minor adjustments (Zhou et al., 2020; Zhao et al., 2021). WFA was intracerebroventicularly administered once daily for 7 days, beginning immediately after ICH surgery. To assess the function of WFA in the brain more directly, we chose the intracerebroventricular injection approach. The experimental timeline and flow chart are shown in **Figures 1** and **2**. For quantitative real-time PCR studies, mice (sham, ICH and WFA 1 μg/kg groups, n = 4 per group) were sacrificed on days 1 and 3 after ICH. The remaining mice were examined by behavioral tests on day 7 and sacrificed for (1) HO-1, Nrf2, β-actin and histone H3 protein quantification assay (n = 6 mice/group); (2) HO-1 mRNA quantification assay (n = 4 mice/group); the brain tissue samples came from the same batch; (3) superoxide dismutase (SOD), GPx and MDA quantification assay (n = 4 mice/group); and (4) Nissl staining and Perl's (Prussian blue) staining (n = 3 mice/group). Experimenters were blinded to experimental conditions during animal modeling, behavioral tests, and histological evaluation.

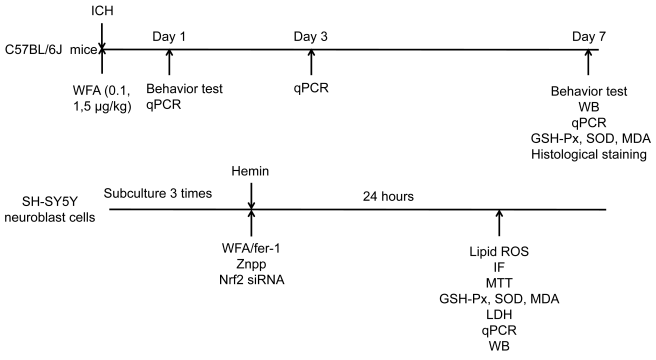

Figure 1 | **Timeline of experimental treatments and model design.**
GSH-Px: Glutathione peroxidase; HO-1: heme oxygenase-1; ICH: intracerebral hemorrhage; IF: immunofluorescence; LDH: lactate dehydrogenase; MDA: malondialdehyde; MTT: 3-(4,5-dimethylthiazol-2-yl)-2,5-diphenyltetrazolium bromide; Nrf2: nuclear factor E2-related factor 2; qRT-PCR: quantitative reverse transcription-polymerase chain reaction; ROS: reactive oxygen species; SOD: superoxide dismutase; WB: western blot; WFA: withaferin A.

ICH models

The ICH mouse model was established by injection of autologous blood into the caudate nucleus as described in a previous report (Diao et al., 2020). Briefly, the mice were anesthetized with 2% sevoflurane with a small animal anesthetic machine (1 L/minute; RWD Life Science, Shenzhen, China) and then attached to a stereotaxic brain locator. Blood from the tail artery (30 μL) was inserted into the right basal ganglia (coordinates: 0.1 mm anterior, 1.0 mm posterior, and 3.0 mm depth) at a rate of 2 μL/minute using a microinfusion pump (RWD Life Science) following a previous report (Diao et al., 2020). The autologous blood came from the tail artery in mice with no anticoagulants. The needle was held in place for a further 10 minutes after the infusion, and the wound was closed. For the sham group, 30 μL of 0.9% saline was injected into the right basal ganglia instead of tail artery blood. A rapid neurological deficiency score was determined using the Garcia test after post-operative recovery. Mice with moderate neurological deficiency were included in this study.

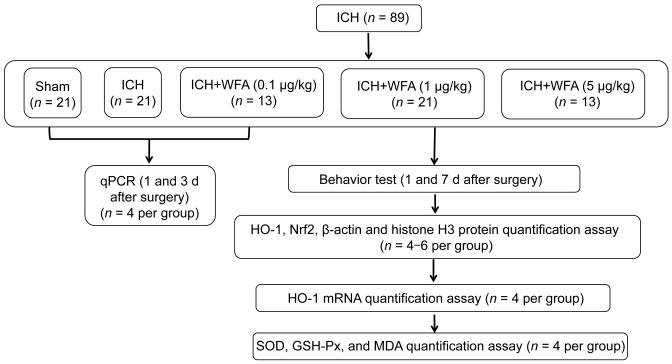

Figure 2 | **The flow chart summarizing experimental setup and the number of mice analyzed at different stages of the study.**
GSH-Px: Glutathione peroxidase; HO-1: heme oxygenase-1; ICH: intracerebral hemorrhage; IF: immunofluorescence; LDH: lactate dehydrogenase; MDA: malondialdehyde; Nrf2: nuclear factor E2-related factor 2; qPCR: quantitative polymerase chain reaction; SOD: superoxide dismutase; WFA: withaferin A.

For cell models of ICH, hemin-induced cell death was used as the *in vitro* ICH model as described (Zille et al., 2017). SH-SY5Y neuroblast cells (Identifier: CSTR: 19375.09.3101HUMSCSP5014, the Type Culture Collection of the Chinese Academy of Sciences, Shanghai, China) were cultured at 37°C with 5% CO_2 in Dulbecco's modified Eagle's medium (DMEM, Gibco, MA, USA), 10% FBS (Gibco), and 1% penicillin/streptomycin (4 mg/mL; Sigma-Aldrich). Cells were seeded in plates for 24 hours and then exposed to 100 μM hemin (BCBR5047V, Sigma-Aldrich) to induce cell death. SH-SY5Y neuroblasts with viability that was reduced by approximately 50% were included in this study.

Grid walking test

The grid walking test was performed on days 1 and 7 after ICH. A 12 mm^2 wire mesh with a grid area of 32 cm × 20 cm × 50 cm was manufactured for the grid-walking task (Chao et al., 2012). The foot faults were assessed using a video camera positioned beneath the device. Mice were placed on the top of the elevated wire grid and were able to move freely until at least 100 steps were taken by the left forelimb. Analysis was performed offline by a rater blind to group design. The total number of step errors (foot errors) and non-foot errors for each limb were counted. If a step provided no support and the foot passed through the hole of the grid, it was considered a fault. A step was also considered a foot fault if an animal was resting with the grid at the level of the wrist. The ratio of foot faults to the total number of steps was calculated as follows: [number of foot faults/(foot faults + number of non-foot fault steps)] × 100%.

Rotarod test

The rotarod test (Liao et al., 2019) was performed on days 1 and 7 after ICH to evaluate motor balance and coordination in mice. Mice were pretrained on an accelerating rotarod cylinder (Xinruan Instruments, Shanghai, China) at a speed of four rotations per minute (r/minute) and then the speed increased gradually to 40 r/minute over 90 seconds. For testing, mice were placed on the rotarod cylinder; the speed was gradually increased from 0 to 40 r/minute within 5 minutes. During the procedure, the latency to falling was recorded.

CatWalk test

The CatWalk test (Domin et al., 2018) was performed on days 1 and 7 after ICH using an automated gait analysis system (walking track test, Xinruan Instruments). The CatWalk system included a closed glass bridge and a camera to record speed. Gait performance was assessed using recording, paw print heat map, and analysis software. For the first 2 days, the mice were allowed to get used to the apparatus for 10 minutes each day. On the next day, free runs were recorded on the walkway. The percentage of correct steps, paw area, and moving speed were collected for analysis. Correct steps referred to a complete and uninterrupted crossing of the walkway and a minimum of nine step sequences. Moving speed was defined as the speed exerted by the paw not in contact with the glass plate.

Histological staining

Mice were infused with saline followed by 4% of paraformaldehyde on day 7 after ICH. The brains were isolated and fixed in 4% paraformaldehyde overnight. The brains were dehydrated with 30% sucrose and then cut into 20 μm-thick slices using a cryostat (Cryostar NX50, Thermo Scientific, MA, USA). Routine Nissl staining (G1436, Beijing Solarbio Science & Technology Co., Ltd., Beijing, China) was performed to examine mouse models of ICH as described in our previous report (Diao et al., 2020). Surviving neurons with pale nuclei and large cell bodies were counted and averaged. Dark-stained neurons and those with shrunken cell bodies were considered dead and were not counted. The tissue sections were stained for ferric iron deposition with the Perl's staining stain kit (G1424, Beijing Solarbio Science & Technology Co., Ltd.) following the manufacturer's instructions. Briefly, tissue sections were moisturized with deionized water, incubated in a Prussian blue solution for

30 minutes, and then washed with deionized water. The sections were then counterstained with eosin staining solution and then rinsed with deionized water. A microscope was used to obtain images (Leica DM2500, Leica Co., Heidelberg, Germany). The positive particles represent the degree of iron deposition.

Malondialdehyde, total superoxide dismutase and GPx activity measurements *in vivo* and *in vitro*

ELISA detection kits for total superoxide dismutase (SOD, S0103, Beyotime Institute of Biotechnology, Nantong, China), total glutathione peroxidase (GPx, S0058, Beyotime Institute of Biotechnology), and malondialdehyde (MDA, S0131S, Beyotime Institute of Biotechnology) were used for measurements. Assays were performed following the manufacturer's instructions. The brain tissues were isolated on day 7 and placed in 0.9% cold saline. Samples were homogenized and centrifuged at 3000 r/minute for 15 minutes. The supernatant was collected for ELISA, and samples were analyzed using a Synergy™ HT multimode microplate reader (Biotek, Shanghai, China).

To measure MDA, SOD and GPx activities in SH-SY5Y cells, cells were seeded at 1×10^5 cells/well in 96-well plates for 24 hours, followed by co-treatment with 100 μM hemin at various concentrations (1, 10 and 100 nM) of WFA or ferrostatin-1 (fer-1, 10 μM) for 24 hours. The cells were collected using a rubber scraper and centrifuged at 1000 × *g* for 10 minutes at 4°C. Cell pellets were lysed in 500 μL of 5% (w/v) metaphosphoric acid. Cellular lysate was centrifuged at 13,000 × *g* for 5 minutes at 4°C. Supernatants were collected for measurement of GSH-Px, SOD and MDA activities using a Synergy™ HT multimode microplate reader (Biotek).

Lipid ROS *in vitro*

A BODIPY 581/591 C11 (D3861, Invitrogen, Waltham, MA, USA) lipid peroxidation sensor was used to detect ROS as described in previous reports (Li et al., 2017; Ingold et al., 2018). Briefly, SH-SY5Y cells were seeded onto glass slides and treated with hemin alone or in the presence of WFA for 24 hours. Cells were incubated for 30 minutes with 5 μM BODIPY C11 and then washed with PBS three times to remove excess BODIPY C11. Lipid ROS fluorescence images were taken under the fluorescence microscope and green fluorescence intensity was computed using ImageJ software.

MTT assay

SH-SY5Y cells in the exponential growth phase were seeded on flat bottomed 96 well plates at 4×10^4 cells/mL. Cells were treated with PBS, hemin, or hemin with different concentrations of WFA (in these groups, cells were incubated with hemin for 30 minutes followed by administration of WFA) for 24–48 hours. The cells were subsequently incubated with 3-(4, 5-dimethylthiazol-2-yl)-2,5-diphenyl tetrazolium bromide (MTT, 5 mg/mL) for 4 hours in the cell culture incubator. Absorbance values at 490 nm wavelength were measured using a Synergy™ HT multimode microplate reader.

Cell lactate dehydrogenase (LDH) release assay

SH-SY5Y cells were treated with PBS, hemin, or hemin with various concentrations of WFA (the cells were incubated with hemin for 30 minutes followed by WFA administration) for 24 hours. The cell supernatant was collected and measured with a cell LDH kit (Beyotime Biotechnology).

Western blot assay

Brain samples were collected on day 7 after ICH. Brain samples or cell samples were isolated and homogenized within RIPA lysis buffer (P0013B, Beyotime Institute of Biotechnology) following the manufacturer's instruction. Lysates were processed using a nuclear and cytoplasmic protein extraction kit (KGBSP002, KeyGEN Biotech, China). Equal quantities of protein per sample were separated by sodium dodecyl sulfate-polyacrylamide gel electrophoresis (SDS-PAGE) and transferred to a membrane. The membrane was blocked with 5% skimmed milk for 1 hour at room temperature, followed by incubation with the following primary antibodies: rabbit anti-HO-1 (1:1000, AF5393, Affinity Biosciences, Changzhou, China), mouse anti Nrf2 (1:1000, BF8017, Affinity Biosciences), mouse anti-4-HNE (1:1000, MA5-27570, ThermoFisher Scientific, MA, USA), rabbit anti-TF (1:800, DF13383, Affinity Biosciences), rabbit anti-FTH1 (1:1500, DF6278, Affinity Biosciences), rabbit anti-β-actin (1:5000, AF7018, Affinity Biosciences), rabbit anti-histone H3 (1:1000, AF0863, Affinity Biosciences) and rabbit anti-GAPDH (1:5000, AF7021, Affinity Biosciences) at 4°C overnight. The membranes were washed with PBS three times, followed by incubation with anti-mouse IgG (1:10,000, S0002, Affinity Biosciences) or anti-rabbit IgG (1:5000, S0001, Affinity Biosciences) for 1 hour at room temperature. The membranes were processed using an enhanced chemiluminescence detection system (Beyotime Biotech) and evaluated using a Gel Imaging System (C500, Azure Biosystems, Dublin, CA, USA). Protein band intensities were normalized to those of β-actin, GAPDH or histone H3 using Image J software.

Immunofluorescence assay

Brain samples were collected on day 7 after ICH. Brain tissues or cell samples were washed with PBS and permeabilized with 0.1% Triton X-100. Samples were incubated with rabbit anti-HO-1 (1:200, AF5393, Affinity Biosciences) and mouse anti-Nrf2 (1:200; AF0639, Affinity Biosciences) at 4°C overnight. Following PBS washes, the samples were incubated with Alexa Fluor-conjugated secondary antibodies (anti-rabbit 488 or 594, 1:200, A32766, A48284, ThermoFisher Scientific, MA, USA) for 1 hour at room temperature, followed by incubation with 4′,6-diamidino-2-phenylindole (DAPI) for 2 minutes. Images were observed with a fluorescence microscope (Leica DM2500, Leica Co.) and analyzed using ImageJ software (NIH, Bethesda, MD, USA). The allocation signals in the dual-channel overlay images were analyzed with the ImageJ "Co-localization Finder" plugin.

Quantitative reverse transcription-PCR

Brain samples were collected on day 7 after ICH. Total RNA was prepared from brain perihematomal tissue or cultured cells using a total RNA Extractor (Trizol) kit (B511311, Sangon Technology Co., Ltd., China) following the manufacturer's instructions. Total RNA was reverse transcribed with reverse transcriptase (RR037Q, Takara, Japan). qPCR was performed with target-specific primers and SYBR Green reagent (RR820Q, Takara Co., Ltd., Japan). Quantitative polymerase chain reaction (qPCR) was performed in 20 μL with cDNA for 40 amplification cycles in a LightCycler 96 System (Roche, IN, USA). The $2^{-\Delta\Delta CT}$ method (Diao et al., 2022) was used to measure mRNA levels and GAPDH mRNA was used as a reference for normalization. Replications of at least three independent tissue samples or cell cultures were used. **Table 1** shows the primer sequences used in this study.

Table 1 | **Primers for quantitative reverse transcription-PCR**

	Gene	Primer sequence (5'–3')	Accession number	Product size (bp)
Mouse	*Ho-1*	Forward: AAG CCG AGA ATG CTG AGT TCA	NM_010442.2	100
		Reverse: GCC GTG TAG ATA TGG TAC AAG GA		
	Gapdh	Forward: AGG TCG GTG TGA ACG GAT TTG	NM_001289726.1	123
		Reverse: TGT AGA CCA TGT AGT TGA GGT CA		
Human	*HO-1*	Forward: AAG ACT GCG TTC CTG CTC AAC	NM_002133.3	247
		Reverse: AAA GCC CTA CAG CAA CTG TCG		
	GAPDH	Forward: GGA GCG AGA TCC CTC CAA AAT	NM_001256799.3	197
		Reverse: GGC TGT TGT CAT ACT TCT CAT GG		

Gapdh/GAPDH: Glyceraldehyde-3-phosphate dehydrogenase; Ho-1/HO-1: heme oxygenase-1.

RNA interference

Mouse siNrf2-1, siNrf2-2 and siScr were obtained from ThermoFisher Scientific (# AM16708). SH-SY5Y cells/mL in the logarithmic growth phase were plated in a 6-well plate (3×10^6 cells/well) and cultivated overnight. Transfection of siRNAs was performed using Lipofectamine 2000 (Invitrogen, Villebon-sur-Yvette, France) in DMEM following the manufacturer's instructions. The cells were allowed to recover in fresh growth medium for 48 hours for gene silencing and then used in subsequent experiments.

Evaluation of WFA interactive genes

The Comparative Toxicogenomics Database (CTD; http://ctdbase.org/) is a robust public database that provides manually prepared information on chemical-gene/protein interactions. The targets of WFA were retrieved and a total of 58 related genes were retrieved from the CTD database before May 1, 2021.

Identification of genes interacting with HO-1

The HO-1 interacting genes were identified from the online search tool STRING database (STRING, V11.0; https://string-db.org/) that predicts protein-protein interactions. All genes in the WFA interaction genes were used for analysis and a total of 15 genes that directly interacted with HO-1 were found before May 1, 2021. Overlapped genes were visualized by Venn analysis with an online tool (https://bioinformatics.psb.ugent.be/webtools/Venn/).

Statistical analysis

Statistical analysis was conducted using GraphPad Prism 8.0.2 software package (GraphPad Software, USA). All results are presented as the mean ± SEM. Significant differences were analyzed by one-way analysis of variance or two-way analysis of variance with Bonferroni correction for *post hoc* comparisons between multiple experimental groups. $P < 0.05$ was regarded as statistically significant.

Results

WFA induces HO-1 expression and reduces oxidative damage at the late stages of ICH *in vivo*

To evaluate the effect of WFA treatment on HO-1 expression during ICH, HO-1 mRNA expression was evaluated in the brain of ICH model mice following WFA treatment. qPCR results indicated that the expression of HO-1 mRNA gradually increased from day 1 to day 7 in the ICH model mice; compared with the controls, WFA at 1 μg/kg significantly increased the expression of HO-1 only on day 7 following ICH ($P = 0.0095$; **Figure 3A**). We thus selected day 7, the late stage of ICH, for subsequent experiments. To determine the optimal dose for WFA treatment, we performed experiments with various doses of WFA. HO-1 expression protein increased significantly on day 7 in the ICH mouse

model compared with the control (P = 0.0446). WFA resulted in a marked up-regulation of HO-1 protein level, depending on the dose. The doses of 1 μg/kg were more efficacious than the doses of 5 μg/kg and 0.1 μg/kg (**Figure 3B** and **C**). We therefore selected the dose of 1 μg/kg for further experiments.

Previous studies showed that HO-1 activates stress response proteins to reduce oxidative damage (Gorg et al., 2019). To clarify the effect of a high level of HO-1 induced by oxidative stress at late stage of ICH, we assessed the level of representative oxidative stress markers on day 7. The MDA oxidative stress marker in the ICH group was higher than that in the sham group (P < 0.0001), and MDA content was much higher in the ICH + WFA groups compared with the ICH group (all P < 0.0001; **Figure 3D**). We also evaluated the activity of the anti-oxidative stress marker GSH-Px. As shown in **Figure 3E**, GSH-Px activity decreased in the ICH group compared with that the sham group (P < 0.0001) and increased in all ICH + WFA groups compared with the ICH group (P < 0.0001). The anti-oxidative stress marker SOD was higher in the ICH group compared with the sham group (P < 0.0001), and ICH + WFA group showed higher levels than the ICH group (P = 0.0068; **Figure 3F**). These data suggest that WFA may reduce oxidative stress by increasing HO-1 expression at the late stage of ICH.

WFA ameliorates brain injury and reduces neurobehavior deficits after ICH *in vivo*

To verify the anti-oxidative damage effects of WFA, we assessed the pathological changes in the perihematomal region after ICH. Nissl staining was conducted to detect the surviving neural cells around the hematoma. As shown in **Figure 4A**, the amount of $Nissl^+$ cells in perihematomal brain tissue were higher in the WFA group than that in the ICH group. We also examined iron accumulation in the brain perihematomal region by Perl's staining (**Figure 4B**). More iron accumulation was found in the perihematomal region of ICH mice than in sham mice. In contrast, treatment with WFA resulted in smaller accumulation of iron compared with the ICH group.

Inhibition of oxidative stress has a beneficial effect on neurofunction recovery after ICH. Thus, to evaluate the effect of WFA treatment on ICH model mice, neurobehavior tests were performed on day 1 and day 7. As assessed by the foot-fault test for forepaw placing and grasping, serious behavioral deficits of the left forepaw were evident in mice at 7 days after ICH (P < 0.0001) (**Figure 4C**). Notably, animals showed a significant dose-dependent improvement at 7 days after ICH with WFA treatment (ICH *vs*. ICH + WFA 0.1 μg/kg P = 0.0139, ICH + WFA 0.1 μg/kg *vs*. ICH + WFA 1 μg/kg, P = 0.0001). In rotarod tests, ICH mice showed a significantly deceased duration of time maintaining balance on the rod (P < 0.0001; **Figure 4D**). WFA-treated mice (1 μg/kg) exhibited a dramatic increase in the performance of the test (P = 0.0139). Gait impairment was evaluated as the percentage of correct steps, the paw area, and the speed via the Catwalk (**Figure 4E–H**). As shown in **Figure 4F**, the percentage of correct steps decreased in the ICH model mice compared with the sham group (P < 0.0001). Treatment with WFA dose-dependently recovered the percentage of correct steps in ICH mice (P = 0.0012, P = 0.0044). Paw area is the area of the paw in contact with road surface during the motion phase. The paw area in the ICH mice was significantly decreased compared with that of the sham mice (P < 0.0001; **Figure 4G**). However, the paw area of ICH mice dose-dependently increased after treatment with WFA (P = 0.0474). Run speed reflects the crawling ability of mice. As shown in **Figure 4H**, the run speed in the sham group was faster than that in the ICH group (P < 0.0001), but it was highly recovered after treatment with 1 μg/kg WFA (P = 0.0305). We also observed severe behavioral deficits in animals 1 day after ICH (**Figure 4C–H**). WFA treatment had no effect on the neurobehavior test results at 1 day post-ICH.

WFA induces HO-1 expression to attenuate oxidative damage *in vitro*

We next examined the expression of HO-1 using western blot analysis in an SH-SY5Y neuroblast cell model of ICH using hemin exposure after WFA treatment. As shown, WFA alone had no effect on HO-1 expression in normal medium. However, upon ICH stress, a significant increase in HO-1 expression was detected (P < 0.0001; **Figure 5A** and **B**). A further increase in HO-1 level was observed after WFA treatment in a dose-dependent manner (P = 0.0097). Furthermore, the ICH cell model showed a decrease in cell viability (P < 0.0001), which was reversed by administration of WFA at the doses of 10 and 100 nm (P = 0.0390, P = 0.0077; **Figure 5C**). To explore the anti-oxidative effect of WFA, we evaluated GSH-Px, SOD and MDA levels *in vitro*. The MDA level was higher in the hemin group compared with control cells (P < 0.0001), and WFA treatment at the doses of 10 and 100 nM significantly decreased MDA level (P = 0.0256, P = 0.0092; **Figure 5D**). Both GSH-Px activity and SOD level in the hemin group were lower than those in the DMEM group (P = 0.0003, P < 0.0001), while WFA-treated groups exhibited increased levels in a dose-dependent manner (P = 0.0140, P = 0.0039, P = 0.0143; **Figure 5E** and **F**).

WFA induces Nrf2 nuclear translocation to increase HO-1 expression *in vivo* and *in vitro*

To explore the mechanisms underlying the upregulation of HO-1 expression with WFA treatment after ICH, bioinformatics analysis was used to identify the key target(s) of WTA. The comparative toxicogenomic database (CTD) was used to search for genes interacting with WFA, and a total of 58 genes were retrieved. Next, all these genes including HO-1 were used for subsequent analysis and a total of 15 genes that directly interacted with HO-1 were found using the STRING database. Among these genes, the nuclear factor erythroid 2-related factor 2 (NFE2L2) gene overlapped with genes that interact with WFA (**Figure 6A**). Nrf2 is normally sequestered in the cytoplasm and bound to keap1, and it is dissociated from keap1 and subsequently promotes nuclear translocation of Nrf2 under stress (Imai et al., 2021). Thus, the effects of WFA on Nrf2 nuclear translocation during ICH were evaluated. As shown in **Figure 6B** and **C**, while the level of Nrf2 expression showed non-significant changes both in the cytoplasm and nucleus in ICH mice, WFA (1 μg/kg) induced a further reduction of Nrf2 expression in the cytoplasm (P = 0.003) and significant elevation of Nrf2 expression in the nucleus (P = 0.0391); higher Nrf2 expression and predominant Nrf2 nuclear location were observed in response to WFA treatment levels in ICH mice (P < 0.001; **Figure 6D**).

We further investigated the impact of WFA treatment on Nrf2 *in vitro* using the hemin-induced cell injury model. As shown in **Figure 6E–G**, nuclear translocation of Nrf2 increased dose-dependently after WFA treatment for 24 hours in hemin-induced SH-SY5Y neuroblast injury (P = 0.0349). The cytoplasmic fractions of Nrf2 were dose-dependently decreased in hemin-induced SH-SY5Y neuroblast injury after WFA treatment for 24 hours (P = 0.0035). Notably, WFA treatment had no effect on the expression of Nrf2 in the nucleus and cytoplasm in the normal medium (P > 0.05). Similar results were shown in immunofluorescence analysis. The overlays of Nrf2 and DAPI images of the two detection channels were used to generate scatterplots and to calculate the Pearson's correlation coefficient (Rr) and Manders parameter of the two fluorescent signals (Dunn et al., 2011). Rr values > 0.5 or Manders values > 0.6 indicate co-localization. As shown in **Figure 6H–K**, WFA treatment promoted Nrf2 nuclear translocation in hemin-induced SH-SY5Y neuroblast injury in a dose-dependent manner. In contrast, Nrf2 expression showed no changes in cells exposed to 10 nM WFA in normal medium. These findings suggest that WFA promoted the translocation of Nrf2 from the cytosol to the nucleus after ICH.

Nrf2 silencing abrogates the upregulation of WFA on expression of HO-1 and oxidative stress *in vitro*

To further investigate the effect of Nrf2 expression in ICH, SH-SY5Y neuroblast cells were transduced with Nrf2-specific siRNA. Both Nrf2 siRNAs significantly suppressed the expression of Nrf2 (P < 0.0001; **Figure 7A** and **B**). Next, the effect of Nrf2 silencing on the expression of HO-1 was analyzed. As shown in **Figure 7C**, WFA induced HO-1 mRNA expression (P = 0.0058), and silencing Nrf2 expression significantly suppressed HO-1 mRNA (P = 0.0082, P = 0.0145). Furthermore, Nrf2 silencing significantly reduced HO-1 protein levels (P = 0.0016, P = 0.0032; **Figure 7D** and **E**). In addition, the role of Nrf2 in the anti-oxidative effects of WFA against neural injury *in vitro* was investigated. As shown in **Figure 7F**, administration with WFA significantly increased cell viability under the ICH condition (P < 0.0001). Nrf2 silencing with siRNA markedly reversed these results (P < 0.0001, P < 0.0001). We then examined the influence of Nrf2 silencing on oxidative stress after WFA treatment. The level of the oxidative stress marker MDA significantly decrease in WFA-treated cells (P = 0.0060), but silencing Nrf2 attenuated the decrease in the level of MDA (P = 0.0026, P = 0.0166; **Figure 7G**). Furthermore, the levels of the anti-oxidative stress markers GSH-Px and SOD both increased markedly in cells exposed to 10 nM WFA (P = 0.0002, P < 0.0001) and Nrf2 silencing reversed these effects (P = 0.0087, P = 0.0067, P = 0.0007, P = 0.0003; **Figure 7H** and **I**).

WFA induces HO-1 expression to mitigate ferroptosis after ICH *in vitro*

Following ICH, the same series of molecular events is found in oxidative stress and the ferroptosis process, such as lipid peroxidation and ROS (Ren et al., 2021). Therefore, WFA may induce HO-1 expression to attenuate oxidative stress associated with ferroptosis-driven cell death after ICH. In addition, zinc protoporphyrin (ZnPP), a specific HO-1 inhibitor, was used to evaluate the effect of HO-1. HO-1 protein expression after ZnPP treatment is shown in **Figure 8A** and **B**, and the results showed that ZnPP significantly down-regulated HO-1 protein level (P < 0.0001). To date, specific ferroptosis markers have not been identified, but several features can separate ferroptotic cell death from other forms of cellular death (Hadian and Stockwell, 2020; Tang et al., 2021). Thus, we first assessed cell viability and found that WFA treatment markedly favored the survival of SH-SY5Y neuroblast in response to hemin-induced injury (P = 0.0484) but was reversed following ZnPP treatment (P = 0.0376; **Figure 8C**). Next, lipid peroxidation was determined by evaluating lipid ROS and 4-HNE. The level of lipid ROS was assessed by BODIPY 581/591 C11 oxidation. Lipid ROS markedly increased in the hemin-induced cell injury model (P = 0.0010) but was restored following WFA treatment (P = 0.0186). ZnPP abrogated this ferroptosis-associated change (P = 0.0204; **Figure 8D** and **E**). We also examined 4-HNE level by western blotting. As shown in **Figure 8F** and **G**, the hemin-induced cell injury model exhibited a highly elevated level of 4-HNE protein compared with controls (P = 0.0057). WFA treatment decreased 4-HNE content to the level in the control group (P = 0.0078). However, inhibition of HO-1 with ZnPP significantly reversed it (P = 0.0063). Next, transferrin (TF) and ferritin (FTH1), key proteins of iron metabolism, were detected by western blotting. As shown in **Figure 8F**, **H** and **I**, the protein level of TF and FTH1 was significantly elevated in the hemin-induced cell injury model (P = 0.0002, P = 0.0006) and WFA decreased both TF and FTH1 expression compared with that in the controls (P = 0.0006, P = 0.0019). Furthermore, inhibition of HO-1 with ZnPP significantly increased TF and FTH1 expression (P = 0.0034, P = 0.0044).

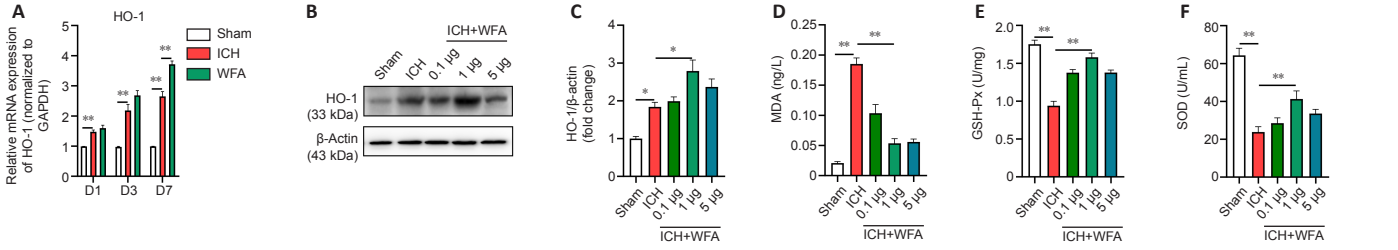

Figure 3 | **Withaferin A (WFA) induces heme oxygenase-1 (HO-1) expression and attenuates oxidative damage in the late stage of intracerebral hemorrhage (ICH) *in vivo*.**
(A) Quantitative analysis of relative gene level of HO-1 in the sham, ICH, and WFA-treated mouse groups on days 1, 3 and 7 after ICH, $^{**}P < 0.01$ (two-way analysis of variance followed by Bonferroni correction). Representative western blot images (B) and quantitative analysis of relative protein levels of HO-1 (C) in the sham, ICH, and ICH + WFA (0.1, 1, and 5 μg/kg) groups on day 7 after ICH. (D) Malondialdehyde (MDA) content in the indicated groups. (E) Glutathione peroxidase (GSH-Px) bioactivity in the indicated groups. (F) Superoxide dismutase (SOD) level in the indicated groups. For B–F, $^{*}P < 0.05$, $^{**}P < 0.01$ (one-way analysis of variance followed by Bonferroni correction). Data are expressed as the mean ± SEM (n = 4). ICH: Intracerebral hemorrhage; WFA: withaferin A.

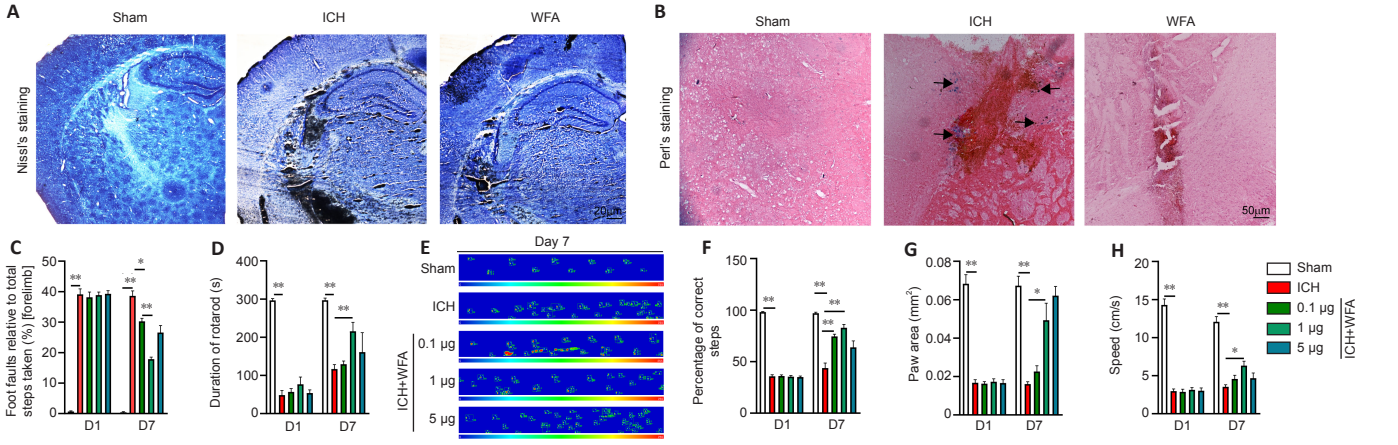

Figure 4 | **WFA improves the pathological changes and decreases the neurobehavioral deficits in the late stage of ICH *in vivo*.**
Pathological changes in mouse brain from the indicated groups were evaluated by Nissl staining (A) and Perl's staining (B) on day 7 after ICH. The blue particles represent the degree of iron deposition and black arrows indicate typical iron deposition. (C) Grid walking test results on days 1 and 7 after ICH. (D) Rotarod test results on days 1 and 7 after ICH. (E) Typical paw prints heat map in each group on day 7 after ICH. Statistical analysis of the percentage of correct steps (F), paw area (G), and speed (H) in each group on days 1 and 7 after ICH. n = 3 mice per group in (A) and (B); n = 10 mice per group in (C–H). $^{*}P < 0.05$, $^{**}P < 0.01$ (two-way analysis of variance followed by Bonferroni correction). Data are expressed as the mean ± SEM. ICH: Intracerebral hemorrhage; WFA: withaferin A.

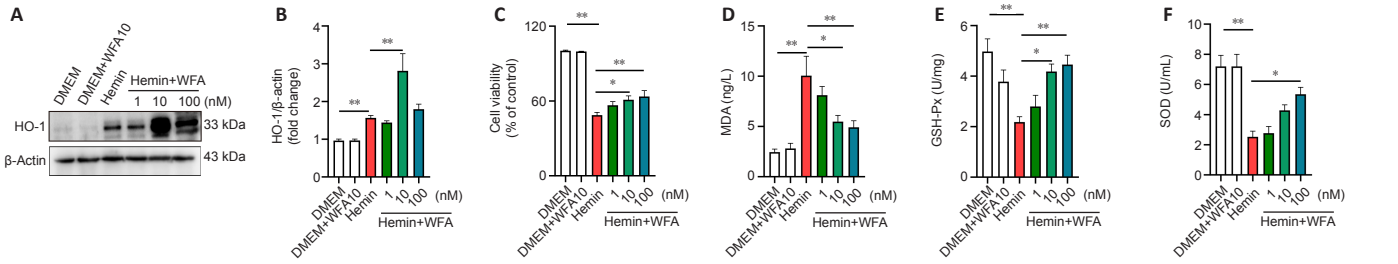

Figure 5 | **WFA induces the expression of HO-1 and prevents oxidative damage in SH-SY5Y neuroblasts *in vitro*.**
Representative western blot images (A) and densitometric analysis (B) of HO-1 expression in SH-SY5Y neuroblasts treated as indicated. Cells were treated with 100 μM hemin alone or co-treated with WFA at various concentrations (1, 10 and 100 nM) for 24 hours. (C) MTT assay was used to analyze cell survival rate in cells treated as indicated. (D) MDA content in the indicated cell groups. (E) GSH-Px bioactivity in the indicated cell groups. (F) SOD level in the indicated cell groups. $^{*}P < 0.05$, $^{**}P < 0.01$ (one-way analysis of variance followed by Bonferroni correction). "ns" stands for non-significant. Data are expressed as the mean ± SEM (n = 6). GSH-Px: Glutathione peroxidase; HO-1: heme oxygenase-1; MDA: malondialdehyde; SOD: superoxide dismutase; WFA: withaferin A.

WFA combined with ferrostatin-1 ameliorates hemin-induced cell injury *in vitro*

To further confirm the causal link between WFA and ferroptosis, ferrostatin-1 (fer-1), a specific ferroptosis inhibitor was used. Cell viability significantly decreased ($P < 0.0001$) and the LDH release significantly increased ($P = 0.0002$) in SH-SY5Y neuroblasts under injury condition. WFA treatment significantly increased SH-SY5Y neuroblast viability ($P = 0.032$) and reduced LDH release to a larger extent ($P = 0.0026$) than that with hemin alone. Moreover, this neuroprotective effect was further enhanced by ferroptosis inhibition following treatment with WFA combined with fer-1 ($P = 0.0055$, $P = 0.0005$; **Figure 9A** and **B**). In addition, the level of lipid ROS markedly increased in hemin-induced SH-SY5Y neuroblast ferroptotic cell death ($P < 0.0001$). The expression of 4-HNE was significantly enhanced after ICH ($P = 0.0008$). WFA treatment prevented the upregulation of lipid ROS ($P = 0.0029$) and 4-HNE ($P = 0.0430$) after ICH. Of note, WFA combined with fer-1 treatment also improved these changes associated with ferroptosis ($P = 0.0002$, $P = 0.0075$; **Figure 9C–F**). We evaluated oxidative damage and the results showed that WFA treatment reduced MDA content ($P = 0.0029$) and increased GSH-Px activity ($P = 0.0133$) after ICH. The combination of WFA and fer-1 further increased this trend ($P = 0.0009$, $P = 0.0137$; **Figure 9G** and **H**).

Discussion

ICH remains a major health issue with high mortality and disability rates (Doria and Forgacs, 2019; Sorensen, 2019). To date, the mechanisms responsible for the onset of ICH remain unclear (Caso and Mosconi, 2021). The pathological mechanisms of the hyperacute (within 3 hours), acute (within 24 hours), and late (after 3 days) stages of ICH can be different. ICH after secondary injury processes including brain edema, neuro-inflammatory, oxidative damage and programmed cell death develops within the first several hours and peaks after 3 days at the late stages of ICH. Both preclinical and clinical studies indicate that the intervention of the above-mentioned pathological mechanisms in the late stage will greatly benefit the prognosis of patients with cerebral hemorrhage (Bobinger et al., 2018; Chen et al., 2020). Previous investigations have indicated that HO-1, a redox-sensitive inducible enzyme, is expressed at low levels under physiological conditions, and stimuli such as bleeding, hypoxia and the inflammatory response can markedly up-regulate its level (Lin et al., 2007; Consoli et al., 2021). In the current study, we found markedly increased expression level of HO-1 in both acute and late stages of ICH. However, HO-1 may exhibit distinct roles in early- and late-stage ICH. Several studies have demonstrated that HO-1 activation relieves brain injury early

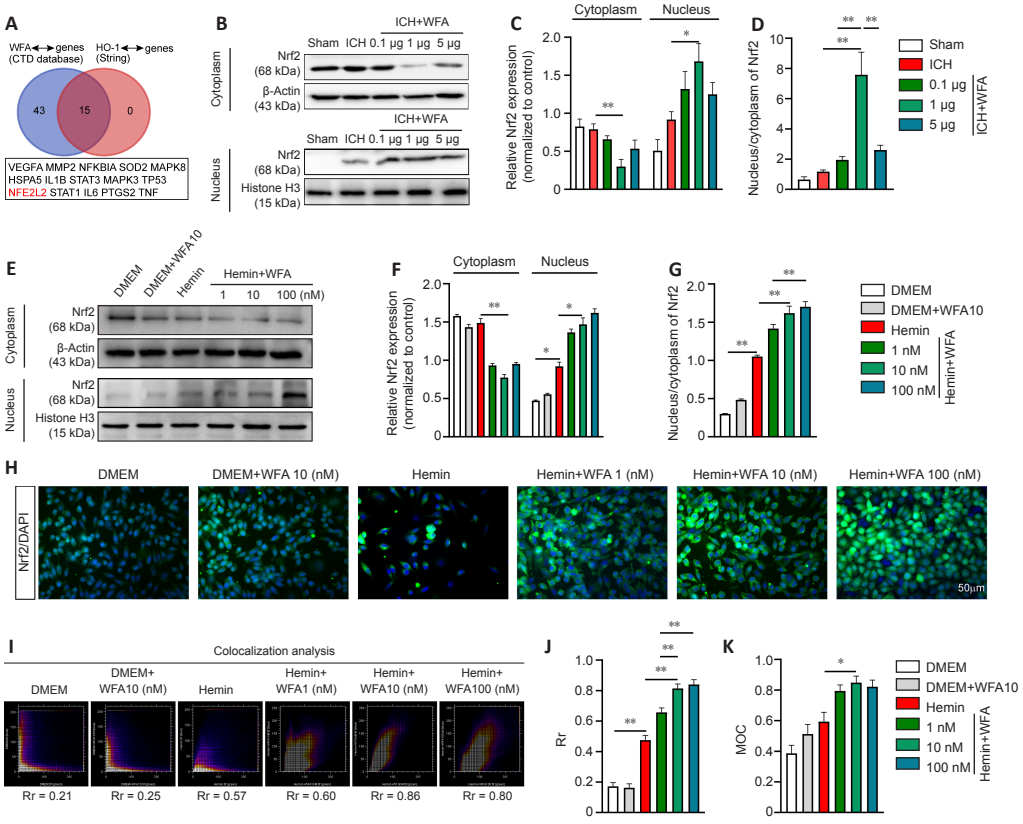

Figure 6 | **WFA upregulates nuclear factor E2-related factor 2 (Nrf2) expression and promotes nuclear translocation of Nrf2 after ICH *in vivo* and *in vitro*.**
(A) Venn analysis of overlapping genes that interact with both WFA and HO-1 in the CTD database and String database. (B) Representative western blot images and (C) quantitative analysis of relative protein level of cytoplasmic Nrf2 and nuclear Nrf2 in the sham, ICH, and WFA (0.1, 1, and 5 μg/kg)-treated groups on day 7 after ICH. (D) Quantification of relative nuclear and cytoplasmic Nrf2 protein levels in the sham, ICH, and WFA (0.1/1/5 μg/kg)-treated groups on day 7 after ICH. (E) Representative western blot images and (F and G) quantification of relative protein expression of cytoplasmic Nrf2, nuclear Nrf2, and ration of nuclear/cytoplasmic Nrf2 in the hemin-induced ICH model with or without WFA treatment. (H) Nrf2 localization was detected by immunofluorescence with an anti-Nrf2 antibody (green fluorescence). Nuclei were stained with DAPI (blue fluorescence). (I) Allocation of green and blue signals in the dual-channel overlay images was analyzed with the ImageJ "Co-localization Finder" plugin, and co-localization of the green and blue signals is shown in white spots. The x-axes indicate the intensities of the green signals from the green channel (Nrf2) and the y-axes from the blue channel (DAPI). For every scatterplot, the intensities are given as the pixel grey values ranging from 0 to 255. Co-localization clusters the pixels from two channels along the diagonal. Pearson's correlation coefficient (Rr) reflects the intensity distribution relationship between the two channels. Manders overlap coefficient (MOC) reflects the true degree of co-localization of the two channels. The maximal theoretical value for the Rr and MOC is 1.0. Quantification analysis of Nrf2 nuclear location with parameter. (J) Pearson's correlation coefficient (Rr) and (K) MOC. n = 6 mice per group in B–D; n = 3 per group in E–K. *P < 0.05, **P < 0.01 (one-way analysis of variance followed by Bonferroni correction). Data are presented as the mean ± SEM. HO-1: Heme oxygenase-1; ICH: intracerebral hemorrhage; Nrf2: nuclear factor erythroid-related factor 2; WFA: withaferin A.

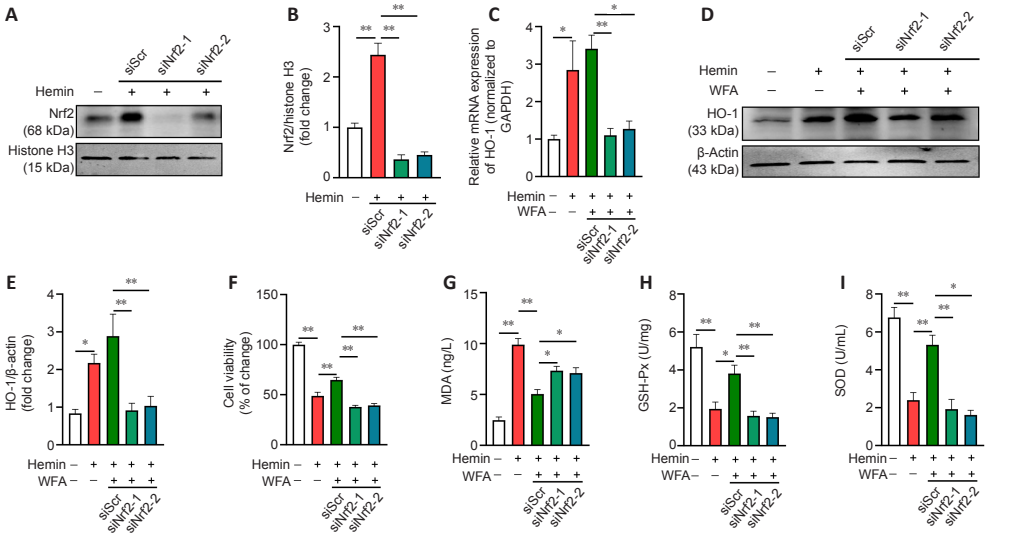

Figure 7 | **Silencing Nrf2 depresses HO-1 expression and reverses WFA protection of hemin-induced SH-SY5Y neuroblast oxidative injury *in vitro*.**
(A) Representative western blot images and (B) quantitative analyses of Nrf2 at 24 hours after siRNA treatment in the ICH injury model induced by hemin with or without WFA exposure. (C) Quantification of relative gene expression of Nrf2 HO-1 after siRNA treatment in the ICH injury model induced by hemin with or without WFA exposure. (D) Representative western blot images and (E) quantitative analyses of HO-1 at 24 hours after siRNA treatment in ICH injury model induced by hemin with or without WFA exposure. (F) Cell survival was analyzed after siRNA treatment in the ICH injury model induced by hemin with or without WFA exposure. (G) MDA content in the indicated groups. (H) GSH-Px activity in the indicated groups. (I) SOD level in the indicated groups. *P < 0.05, **P < 0.01 (one-way analysis of variance followed by Bonferroni correction). Data are expressed as the mean ± SEM (n = 6). GSH-Px: Glutathione peroxidase; HO-1: heme oxygenase-1; MDA: malondialdehyde; Nrf2: nuclear factor erythroid-related factor 2; SOD: superoxide dismutase; WFA: withaferin A.

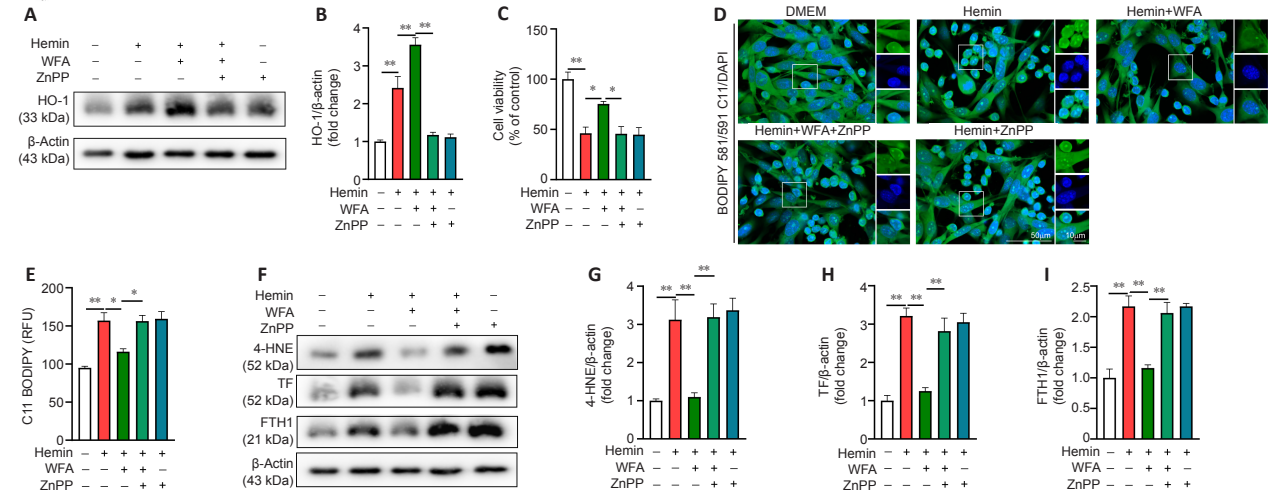

Figure 8 | **WFA induces HO-1 expression, resulting in ameliorated ferroptosis in hemin-induced SH-SY5Y neuroblast injury *in vitro*.**
(A) Representative western blot bands and (B) relative density of HO-1 in different groups. (C) Cell viability detection in different groups. (D) Typical BODIPY 581/591 C11 fluorescence images and (E) fluorescence density of BODIPY 581/591 C11 in different groups. Green indicates lipid ROS and blue indicates nuclei. (F) Representative western blot bands and (G–I) quantification of the relative density of 4-HNE, TF and FTH1 band densities in different groups. *P < 0.05, **P < 0.01 (one-way analysis of variance followed by Bonferroni correction). Data are expressed as the mean ± SEM (n = 3). 4-HNE: 4-Hydroxynonenal; FTH1: ferritin heavy chain 1; HO-1: heme oxygenase-1; TF: transferrin; WFA: withaferin A; ZnPP: zinc protoporphyrin, a specific HO-1 inhibitor.

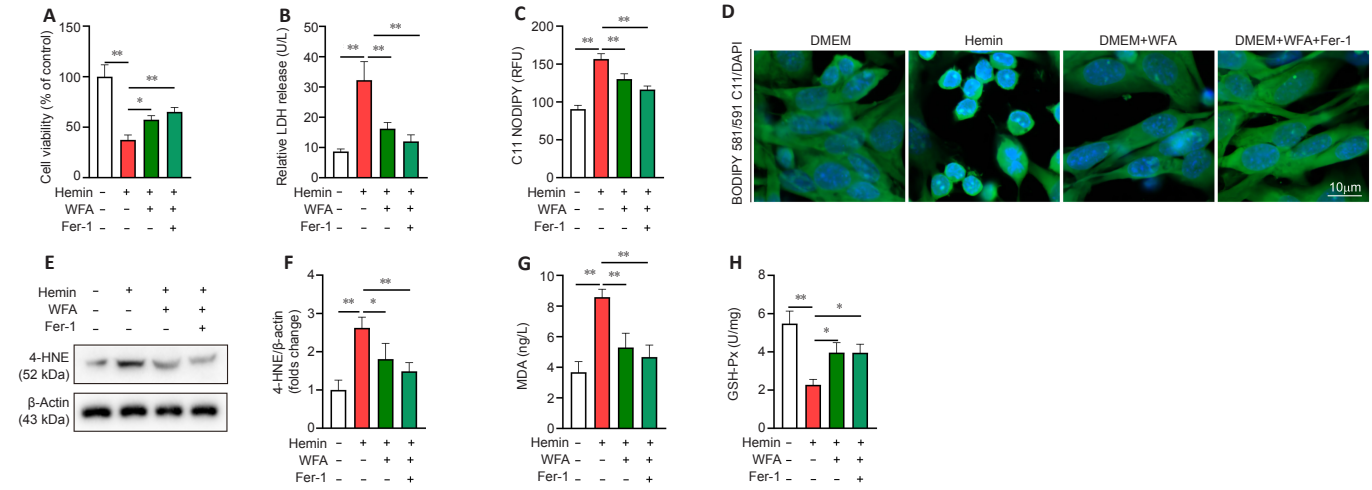

Figure 9 | **WFA combined with ferrostatin-1 influences cell damage in response to hemin-induced cell injury *in vitro*.**
Quantification analysis of cell viability with MTT assay (A) and LDH release (B). (C) Quantification of BODIPY 581/591 C11 fluorescence density. (D) Representative images in the indicated groups. Green indicates lipid ROS and blue indicates nuclei. (E) Representative western blot bands and (F) quantification of the relative density of 4-HNE in the indicated groups. (G) MDA level in the indicated groups. (H) GSH-Px activity in the indicated groups. *P < 0.05, **P < 0.01, between the indicated groups (one-way analysis of variance followed by Bonferroni correction). Data are presented as the mean ± SEM (n = 3). 4-HNE: 4-Hydroxynonenal; Fer-1: ferrostatin-1; GSH-Px: glutathione peroxidase; LDH: lactic dehydrogenase; MDA: malondialdehyde; WFA: withaferin A.

after ICH but promotes neuro-function recovery in the later stage of ICH (Wang and Dore, 2007; Chen-Roetling et al., 2017). Of note, our results showed that WFA only increased HO-1 expression at the late stage of ICH in a dose-dependent manner. Thus, we speculate that WFA may exert neuroprotective effects after ICH by upregulation of HO-1 expression. Furthermore, Choi et al. (2008) reported that HO-I played a marked role in the protection against oxidative tissue injury. Indeed, we found that (1) WFA markedly increased the level of HO-1 following ICH *in vivo* and *in vitro*; (2) up-regulation of MDA content and down-regulation of GSH-Px and SOD activities were markedly reversed by WFA treatment in both *in vivo* and *in vitro* ICH models; and (3) WFA treatment markedly improved the outcomes of ICH both *in vivo* and *in vitro*. Thus, the current findings suggested that WFA exerts its neuroprotective effect by reducing oxidative stress injury after ICH via upregulation of HO-1 level.

Little has been known about the antioxidant mechanism of the neuroprotective effects of WFA. Nrf2 is a key transcription factor that regulates the antioxidant defense system. When exposed to oxidants, cytoplasmic Nrf2 is translocated into the nucleus, where it binds to HO-1 consensus binding sequence to induce its expression. Therefore, WFA may regulate Nrf2/HO-1 pathway to promote its anti-oxidative stress effect after ICH. Therefore, Nrf2 expression was investigated *in vivo* and *in vitro* following WFA treatment. In *in vivo* hemorrhagic stroke, the expression and nuclear localization of Nrf2 were up-regulated after ICH, and nuclear expression was further increased after WFA administration. Similar results were found in SH-SY5Y neuron cell models of ICH (Heyninck et al., 2016). To further identify the critical role of Nrf2/HO-1 pathway in the anti-oxidative stress effect of WFA, Nrf2 siRNA was used to downregulate its expression. The results showed that the upregulation effect of WFA on HO-1 expression was abolished by Nrf2 siRNA. Furthermore, the suppressive effect of WFA on oxidative damage was also markedly inhibited by Nrf2 siRNA. In addition, Nrf2 siRNA reversed the protective effect of WFA on hemin-induced SH-SY5Y neuronal cell injury. Together these results further indicated that WFA protects against ICH by reducing oxidative stress and activating the Nrf2/HO-1 pathway.

Oxidative stress, caused by excessive ROS inducing lipid peroxidation and oxidation of proteins, DNA, and RNA, leads to neuronal dysfunction and death (van der Pol et al., 2019). Ferroptosis is a non-apoptotic, iron-dependent oxidative form of cell death that is involved in the pathogenesis of ICH (Green, 2019; Li et al., 2020). Oxidative stress induces neuronal cell death via tert-butyl hydroperoxide, which can be blocked by ferroptosis inhibitors, implying a crosstalk between the initial oxidative damage and ferroptosis (DeGregorio-Rocasolano et al., 2019). Moreover, the Nrf2/HO-1 pathway plays a pivotal role in ferroptosis (Ma et al., 2020). Therefore, we speculate that WFA activates the Nrf2/HO-1 pathway to play a neuroprotective role in ICH. In addition, it may inhibit neuronal ferroptotic death by suppressing oxidative damage. Our data showed that ICH results in marked elevation of lipid ROS, 4-HNE protein and the key iron metabolism proteins (TF and FTH1), whereas WFA notably decreased their levels. In addition, the HO-1 inhibitor ZnPP reversed the effect of WFA. Thus, the neuroprotective effect of high HO-I expression on WFA may be partly achieved by inhibiting the expression of HO-I.

Zhou et al. (2020) found that WFA suppressed the apoptosis of endothelial cells and modulated microglial activation. Endothelial cell injury and the inflammatory response caused by microglia have also been implicated in ICH pathogenesis. Thus, we cannot exclude the possibility that the anti-inflammatory and anti-apoptotic effects of WFA may have played a role following ICH. In addition, ferroptosis plays a critical role in brain lesions, including stroke and subarachnoid hemorrhage. Therefore, we speculate that WFA, as a ferroptosis inhibitor, plays a role in a broader range of brain diseases through different mechanisms, and these mechanisms need to be explored further.

In conclusion, the present study demonstrated that WFA had a neuroprotective effect and promoted functional recovery after ICH. In both an *in vivo* model and *in vitro* model, WFA application inhibited ferroptosis and attenuated oxidative stress–related damage after hemorrhagic stroke and these effects were at least partially related to enhanced Nrf2 translocation and HO-1 expression. Collectively, our study suggests that WFA may serve as a promising treatment for hemorrhagic stroke.

Acknowledgments: *We thank the members of Laboratory of Neuroscience and Guangxi Clinical Research Center for Neurological Diseases, Affiliated Hospital of Guilin Medical University for the thoughtful discussions and careful animal care.*

Author contributions: *ZXZ and QC performed the experiments, analyzed the data and wrote the paper. YMZ, JXY, WJX and NT contributed to some parts of the experiments. YLJ, MLC, BY and QHL designed the experiment and provided advice on the interpretation of the data. RJL conceived and designed the experiment, analyzed and interpreted the data, and wrote the paper. All authors read and approved the final manuscript.*

Conflicts of interest: *The authors declare that they have no conflict of interest.*

Availability of data and materials: *All data generated or analyzed during this study are included in this published article and its supplementary information files.*

Open peer reviewers: *Xiao Zheng, China Pharmaceutical University School of Pharmacy, China; Lei Zhang; Fifth Affiliated Hospital of Sun Yat-sen University, China.*

Additional file:

Additional file 1: *Open peer review reports 1 and 2.*

References

Bai Q, Liu J, Wang G (2020) Ferroptosis, a regulated neuronal cell death type after intracerebral hemorrhage. Front Cell Neurosci 14:591874.

Bao WD, Zhou XT, Zhou LT, Wang F, Yin X, Lu Y, Zhu LQ, Liu D (2020) Targeting miR-124/Ferroportin signaling ameliorated neuronal cell death through inhibiting apoptosis and ferroptosis in aged intracerebral hemorrhage murine model. Aging Cell 19:e13235.

Bobinger T, Burkardt P, B Huttner H, Manaenko A (2018) Programmed Cell Death after Intracerebral Hemorrhage. Curr Neuropharmacol 16:1267-1281.

Caso V, Mosconi MG (2021) Lessons to be learned in intracerebral haemorrhage research. Lancet Neurol 20:779-780.

Chao OY, Pum ME, Li JS, Huston JP (2012) The grid-walking test: assessment of sensorimotor deficits after moderate or severe dopamine depletion by 6-hydroxydopamine lesions in the dorsal striatum and medial forebrain bundle. Neuroscience 202:318-325.

Chau LY (2015) Heme oxygenase-1: emerging target of cancer therapy. J Biomed Sci 22:22.

Chen-Roetling J, Kamalapathy P, Cao Y, Song W, Schipper HM, Regan RF (2017) Astrocyte heme oxygenase-1 reduces mortality and improves outcome after collagenase-induced intracerebral hemorrhage. Neurobiol Dis 102:140-146.

Chen B, Chen Z, Liu M, Gao X, Cheng Y, Wei Y, Wu Z, Cui D, Shang H (2019a) Inhibition of neuronal ferroptosis in the acute phase of intracerebral hemorrhage shows long-term cerebroprotective effects. Brain Res Bull 153:122-132.

Chen C, Cui J, Ji X, Yao L (2020) Neuroprotective functions of calycosin against intracerebral hemorrhage-induced oxidative stress and neuroinflammation. Future Med Chem 12:583-592.

Chen S, Wang X, Nisar MF, Lin M, Zhong JL (2019b) Heme oxygenases: cellular multifunctional and protective molecules against UV-induced oxidative stress. Oxid Med Cell Longev 2019:5416728.

Choi KM, Gibbons SJ, Nguyen TV, Stoltz GJ, Lurken MS, Ordog T, Szurszewski JH, Farrugia G (2008) Heme oxygenase-1 protects interstitial cells of Cajal from oxidative stress and reverses diabetic gastroparesis. Gastroenterology 135:2055-2064, 2064.e1-e2.

Collaborators GBDS (2021) Global, regional, and national burden of stroke and its risk factors, 1990-2019: a systematic analysis for the Global Burden of Disease Study 2019. Lancet Neurol 20:795-820.

Consoli V, Sorrenti V, Grosso S, Vanella L (2021) Heme oxygenase-1 signaling and redox homeostasis in physiopathological conditions. Biomolecules 11:589.

DeGregorio-Rocasolano N, Marti-Sistac O, Gasull T (2019) Deciphering the iron side of stroke: neurodegeneration at the crossroads between iron dyshomeostasis, excitotoxicity, and ferroptosis. Front Neurosci 13:85.

Diao X, Cui Q, Tian N, Zhou Z, Xiang W, Jiang Y, Deng J, Liao H, Lin X, Li Q, Liao R (2022) Hemorrhage-induced sphingosine kinase 1 contributes to ferroptosis-mediated secondary brain injury in intracerebral hemorrhage. Mol Neurobiol 59:1381-1397.

Diao X, Zhou Z, Xiang W, Jiang Y, Tian N, Tang X, Chen S, Wen J, Chen M, Liu K, Li Q, Liao R (2020) Glutathione alleviates acute intracerebral hemorrhage injury via reversing mitochondrial dysfunction. Brain Res 1727:146514.

Domin H, Przykaza L, Kozniewska E, Boguszewski PM, Smialowska M (2018) Neuroprotective effect of the group III mGlu receptor agonist ACPT-I after ischemic stroke in rats with essential hypertension. Prog Neuropsychopharmacol Biol Psychiatry 84:93-101.

Doria JW, Forgacs PB (2019) Incidence, implications, and management of seizures following ischemic and hemorrhagic stroke. Curr Neurol Neurosci Rep 19:37.

Dunn KW, Kamocka MM, McDonald JH (2011) A practical guide to evaluating colocalization in biological microscopy. Am J Physiol Cell Physiol 300:C723-C742.

Feigin VL, Vos T, Nichols E, Owolabi MO, Carroll WM, Dichgans M, Deuschl G, Parmar P, Brainin M, Murray C (2020) The global burden of neurological disorders: translating evidence into policy. Lancet Neurol 19:255-265.

Fernandez-Mendivil C, Luengo E, Trigo-Alonso P, Garcia-Magro N, Negredo P, Lopez MG (2021) Protective role of microglial HO-1 blockade in aging: implication of iron metabolism. Redox Biol 38:101789.

Gorg B, Karababa A, Schutz E, Paluschinski M, Schrimpf A, Shafigullina A, Castoldi M, Bidmon HJ, Haussinger D (2019) O-GlcNAcylation-dependent upregulation of HO1 triggers ammonia-induced oxidative stress and senescence in hepatic encephalopathy. J Hepatol 71:930-941.

Green DR (2019) The coming decade of cell death research: five riddles. Cell 177:1094-1107.

Hadian K, Stockwell BR (2020) SnapShot: Ferroptosis. Cell 181:1188.e1.

Heyninck K, Sabbe L, Chirumamilla CS, Szarc Vel Szic K, Vander Veken P, Lemmens KJ, Lahtela-Kakkonen M, Naulaerts S, Op de Beeck K, Laukens K, Van Camp G, Weseler AR, Bast A, Haenen GR, Haegeman G, Vanden Berghe W (2016) Withaferin A induces heme oxygenase (HO-1) expression in endothelial cells via activation of the Keap1/Nrf2 pathway. Biochem Pharmacol 109:48-61.

Imai T, Matsubara H, Hara H (2021) Potential therapeutic effects of Nrf2 activators on intracranial hemorrhage. J Cereb Blood Flow Metab 41:1483-1500.

Ingold I, Berndt C, Schmitt S, Doll S, Poschmann G, Buday K, Roveri A, Peng X, Porto Freitas F, Seibt T, Mehr L, Aichler M, Walch A, Lamp D, Jastroch M, Miyamoto S, Wurst W, Ursini F, Arnér ESJ, Fradejas-Villar N, et al. (2018) Selenium utilization by GPX4 Is required to prevent hydroperoxide-induced ferroptosis. Cell 172:409-422.e1.

Li J, Cao F, Yin HL, Huang ZJ, Lin ZT, Mao N, Sun B, Wang G (2020) Ferroptosis: past, present and future. Cell Death Dis 11:88.

Li Q, Han X, Lan X, Gao Y, Wan J, Durham F, Cheng T, Yang J, Wang Z, Jiang C, Ying M, Koehler RC, Stockwell BR, Wang J (2017) Inhibition of neuronal ferroptosis protects hemorrhagic brain. JCI Insight 2:e90777.

Liao R, Chen Y, Cheng L, Fan L, Chen H, Wan Y, You Y, Zheng Y, Jiang L, Chen Z, Zhang X, Hu W (2019) Histamine H1 receptors in neural stem cells are required for the promotion of neurogenesis conferred by h3 receptor antagonism following traumatic brain injury. Stem Cell Rep 12:532-544.

Lin Y, Vreman HJ, Wong RJ, Tjoa T, Yamauchi T, Noble-Haeusslein LJ (2007) Heme oxygenase-1 stabilizes the blood-spinal cord barrier and limits oxidative stress and white matter damage in the acutely injured murine spinal cord. J Cereb Blood Flow Metab 27:1010-1021.

Ma H, Wang X, Zhang W, Li H, Zhao W, Sun J, Yang M (2020) Melatonin suppresses ferroptosis induced by high glucose via activation of the Nrf2/HO-1 signaling pathway in type 2 diabetic osteoporosis. Oxid Med Cell Longev 2020:9067610.

Ren JX, Li C, Yan XL, Qu Y, Yang Y, Guo ZN (2021) Crosstalk between oxidative stress and ferroptosis/oxytosis in ischemic stroke: possible targets and molecular mechanisms. Oxid Med Cell Longev 2021:6643382.

Sorensen HT (2019) Global burden of neurological disorders: challenges and opportunities with the available data. Lancet Neurol 18:420-421.

Tang D, Chen X, Kang R, Kroemer G (2021) Ferroptosis: molecular mechanisms and health implications. Cell Res 31:107-125.

van der Pol A, van Gilst WH, Voors AA, van der Meer P (2019) Treating oxidative stress in heart failure: past, present and future. Eur J Heart Fail 21:425-435.

Wan J, Ren H, Wang J (2019) Iron toxicity, lipid peroxidation and ferroptosis after intracerebral haemorrhage. Stroke Vasc Neurol 4:93-95.

Wang J, Dore S (2007) Heme oxygenase-1 exacerbates early brain injury after intracerebral haemorrhage. Brain 130:1643-1652.

Xie J, Hong E, Ding B, Jiang W, Zheng S, Xie Z, Tian D, Chen Y (2020) Inhibition of nox4/ros suppresses neuronal and blood-brain barrier injury by attenuating oxidative stress after intracerebral hemorrhage. Front Cell Neurosci 14:578060.

Xue M, Yong VW (2020) Neuroinflammation in intracerebral haemorrhage: immunotherapies with potential for translation. Lancet Neurol 19:1023-1032.

Yang YY, Wang JF, Zhang HY, Wang YW, Yang SQ (2016) Bone marrow mononuclear cell transplantation for cerebral hemorrhage. Zhongguo Zuzhi Gongcheng Yanjiu 20:2831-2837.

Yin XP, Chen ZY, Zhou J, Wu D, Bao B (2015) Mechanisms underlying the perifocal neuroprotective effect of the Nrf2-ARE signaling pathway after intracranial hemorrhage. Drug Des Devel Ther 9:5973-5986.

Zhang Z, Song Y, Zhang Z, Li D, Zhu H, Liang R, Gu Y, Pang Y, Qi J, Wu H, Wang J (2017) Distinct role of heme oxygenase-1 in early- and late-stage intracerebral hemorrhage in 12-month-old mice. J Cereb Blood Flow Metab 37:25-38.

Zhao M, Wang B, Zhang C, Su Z, Guo B, Zhao Y, Zheng R (2021) The DJ1-Nrf2-STING axis mediates the neuroprotective effects of Withaferin A in Parkinson's disease. Cell Death Differ 28:2517-2535.

Zhou Z, Xiang W, Jiang Y, Tian N, Wei Z, Wen X, Wang W, Liao W, Xia X, Li Q, Liao R (2020) Withaferin A alleviates traumatic brain injury induced secondary brain injury via suppressing apoptosis in endothelia cells and modulating activation in the microglia. Eur J Pharmacol 874:172988.

Zille M, Karuppagounder SS, Chen Y, Gough PJ, Bertin J, Finger J, Milner TA, Jonas EA, Ratan RR (2017) Neuronal death after hemorrhagic stroke in vitro and in vivo shares features of ferroptosis and necroptosis. Stroke 48:1033-1043.

P-Reviewers: Zheng X, Zhang L; C-Editor: Zhao; S-Editors: Wang J, Li CH; L-Editors: Wolf GW, Song LP; T-Editor: Jia Y